Evidence of electronic structural change at the metal-insulator transition in the perovskite math xmlns="http://www.w3.org/1998/Math/MathML">mrow>mi >NaOs/mi>msub>mi mathvariant="normal">O/mi> mn>3/mn>/msub>/mrow>/math>

J.-S. Zhou, X.-Y. Li, and M. D. Johannes

Phys. Rev. B **108**, 195115 — Published 8 November 2023

DOI: 10.1103/PhysRevB.108.195115

Evidence of electronic structural change at metal-insulator transition in the perovskite $NaOsO_3$

J.-S. Zhou[1]*, X.-Y. Li[1], M.D. Johannes[2]

[1]Materials Science and Engineering Program, Mechanical Engineering, University of Texas at Austin, Austin, TX 78712.

[2] Center for Computational Materials Science, Naval Research Laboratory, Washington D.C. 20375

$NaOsO_3$ exhibits an unusual metal-insulator transition (MIT), that has been touted as Slater-type, though there are observations that do not entirely conform to this typing. Consistent with a Slater transition, the cell volume and the crystal symmetry show no change on cooling through the transition, but both *a* and *b* axes in this *Pbnm* orthorhombic perovskite show a clear kink and the splitting between them enlarges slightly. Since atomic positions, determined by fitting the intensity of state-of-the-art neutron diffraction data, exhibit no anomalies within the measurement uncertainty, the origin of the *a*-*b* splitting and the kink in the data have not yet been elucidated. Understanding the origin of these subtle structural changes across the transition temperature may help provide understanding about the electronic behavior. In this study, we connect local structural changes to changes in the lattice parameters through (1) well-established structural modelling and (2) density functional theory (DFT) calculations. This approach successfully reveals a subtle, but significant change of the O-Os-O bond angle on cooling through T_{MIT}. A Madelung energy calculation suggests that this bond angle change signals electron localization in the t_{2g} orbital complex and this is verified by DFT which shows an electronic transition from itinerant to localized electronic behavior along with the bond angle shift. This detailed structural study adds an important, though heretofore overlooked, element in the microscopic picture of the metal-insulator transition in $NaOsO_3$.

I. Introduction

$NaOsO_3$ undergoes a sharp metal-insulator transition (MIT) at T_{MIT}= 410 K [1], accompanied by a long range colinear G-type antiferromagnetic ordering with a moment of ~1.0 μ_B on Os^{5+}, as measured by neutron diffraction [2]. Above the transition temperature, $NaOsO_3$ is a metal with resistivity at the level of 10^{-4} Ω cm and a weak temperature dependence. Fitting the magnetic susceptibility $\chi(T)$ to a Curie-Weiss law gives rise to a μ_{eff}=2.7 μ_B, nearly three times the observed moment in the magnetically ordered phase below T_{MIT}, and an unphysically large Weiss constant Θ = -1949 K. On cooling through T_{MIT}, the magnetization jumps in the same way as in other antiferromagnets with canted spins[3,4] and the resistivity has a sharp jump followed by an increase of over 10^7 orders of magnitude as cooling continues to the lowest temperature. Although tremendous efforts have been made, a sound understanding of this seemingly simple transition remains elusive.

As indicated by high resolution neutron diffraction [2], there are no changes in the structural symmetry or cell volume upon crossing the transition temperature, with the observed jump in resistivity apparently related only to the AF spin ordering. The combination of chemical sensitivity of absorption and the atomic position sensitivity of diffraction offered by RIXS can accurately determine electron density in OsO_6 octahedra in both the insulating and metallic states of $NaOsO_3$. Consistent with the neutron diffraction study, the RIXS study[5] also shows no symmetry change from the isosurface of the 5d electron density of Os ions upon crossing T_{MIT}. These observations together with a smaller magnetic moment than that expected from localized t_{2g}^3 electrons on Os^{5+} have lead authors to the conclusion that the metal-insulator transition in $NaOsO_3$ is a case of the rare Slater metal-insulator transition where a gap at the Fermi energy opens as electrons are scattered differently at the two sublattices of the AF ordered magnetic structure [6]. An IR spectroscopy study [7] indeed revealed the formation of a gap Δ(T) that can be fit well to the BCS theory below T_{MIT}, which implies a band electronic state remains in the insulating state and is consistent with the Slater MIT. However, other RIXS studies [8] [9] offer evidence of correlation fluctuations in the metallic phase above T_{MIT}, which is clearly incompatible with the mean-field treatment used in the Slater mechanism.

Band structure calculations[10] indicate that the electronic structure near the Fermi energy is dominated by hybridized Os:5d and O:2p states formed by the $pd\pi^*$ (t_{2g}) with the $pd\sigma^*$ (e_g) complex gapped away by ~ 1eV in the experimental structure. The application of a Hubbard U in the non-magnetic or ferromagnetic state does not lead to a gap opening at the Fermi energy, even for large values of U. The addition of a spin-orbit coupling (SOC) term also does precipitate a gap opening or affect the atomic or lattice parameters, likely because the orbital angular momentum is quenched for the t_{2g}^3 orbital occupation in $NaOsO_3$. Kim *et al.*[11] have shown that SOC *is* a key parameter in controlling the balance between the on-site Coulomb repulsion U and the bandwidth W. In this situation, the correct G-type spin ordering, along with an applied U, separates the two connected bands as described in a Lifshitz transition. Jung *et al.*[12] have shown that no magnetic ordering of *any type* can be obtained in the cubic cell within ±3% variation of the experimental volume. Thus, both octahedral tilting and application of a U are necessary to achieve a full gap at the Fermi energy in the G-type AFM state. The tilting additionally further splits the $pd\pi$ and $pd\sigma$ complexes but narrows the bandwidths. With any additional tilting of the octahedra beyond a critical threshold, the moment on Os^{5+} drops below the observed value. All of these observations are broadly consistent with a Slater transition picture. It should be noted that none of these band models can account for the high Néel transition temperature observed in $NaOsO_3$. While this is readily solved by a calculation based on the Hubbard model, there is no experimental evidence to support the characteristically localized electrons of this model in the magnetically ordered state [13].

In this work, we revisit density functional theory (DFT) calculations in the context of sensitive neutron diffraction data and structural models, employing both full structural relaxations and electronic structure results to tie an overlooked but important O_{21}-Os-O_{22} bond angle α (see Fig.1) to electronic localization. We begin by noting that, although the symmetry and volume do not change across the transition, the *a* and *b* lattice parameters change abruptly in opposite directions, preserving the volume. We argue that these changes are explained by a change in the bond angle, α, and that α is established by a balance between a universal structural distortion in the orthorhombic perovskites [14] that shifts the value of α away from 90° and the preference for

α=90° for localized electrons in the t_{2g} orbital. Thus, the transition is characterized by a shift from itinerant to localized paradigms.

II. Experimental observations and crystallographic model

The *Pbnm* structure is the most popular one in the perovskite family ABX_3 and can accommodate rich structural distortions away from cubic, including the tilting and rotation of octahedra, bond length splitting, and angular octahedral distortion. In 3d transition metal perovskites, it has been theoretically shown that the metal-insulator transition is coupled closely to these cooperative elastic fluctuations [15] and a Mott-Hubbard transition has been widely found to be first order with the long-range magnetic ordering sometimes coincident and sometimes following at a lower temperature [16]. A canonical example is the perovskite $RNiO_3$ (R = rare earth) [17 18 19] . A strong first-order MIT has T_N=T_{MIT} for R=Pr, Nd and $T_N < T_{MIT}$ for the smaller rare earths. The highest occupied electronic states are in the $pd\sigma$* manifold and the electronic-state change from itinerant to localized behavior is accompanied by a change of the cell volume.

In $NaOsO_3$, no change in atomic positions or electron density are observed upon crossing the metal-insulator transition within the resolution of state-of-the-art experiment [2 5]. However, the lattice changes in response to an electronic-state transition are expected to be more subtle for the low-spin 5d electronic state where the wavefunction is more extended than in 3d or 4d systems. Although atomic positions determined by fitting the peak intensity of neutron diffraction entail considerable uncertainty, the angle-resolved diffraction used for calculating lattice parameters provides much more accuracy (to seven or eight significant figures). This suggests that, by extracting local structure from the lattice parameters through careful structural models, a meaningful correlation can be made between necessarily small local structural changes and any electronic transitions that accompany them. With this construct in mind, we concentrate on a specific subtle change in OsO_6 octahedra upon crossing T_{MIT} via a thorough structural analysis, and explicate its relevance for the electronic state in $NaOsO_3$. Whereas the cell volume reported does not show any discernible changes on crossing T_{MIT}, the *a* and *b* axes in the structure with the *Pbnm* setting, change dramatically as shown in Fig.2. The relevance of these lattice parameter changes at T_{MIT} has been largely ignored by both experimental and theoretical groups and its impact on electronic aspects has not been explored.

The *Pbnm* distortion away from the cubic *Pm-3m* structure occurs because of the bonding mismatch for the geometric tolerance factor $t \equiv (A-X)/\sqrt{2}(B-X) < 1$ in a perovskite ABX_3 compound. In oxides, the distortion is a $GdFeO_3$-type orthorhombic distortion in which the octahedral tilting system is described by a primary octahedral-site rotation φ, see Fig.1(b). Lattice parameters can be derived from φ through the formula given by O'Keeffe and Hyde. [20]

$$a = d\sqrt{8}\cos\varphi,\ b = d[8(2 + \cos^2\varphi)/3]^{1/2},\ c = d[48/(1+2\sec 2\varphi)]^{1/2}, \quad (1)$$

where *d* is the *B-X* bond distance. The primary rotation φ can be determined by the atomic positions, for example, from X" in 8(d) (x,y,z), *i.e.* O_{21} or O_{22} in Fig.1(a).

$$x = (3\sqrt{3} + \tan\varphi)/\sqrt{48},\ y = (2-\sqrt{3}\sin\varphi\cos\varphi + \cos^2\varphi)/(8+4\cos^2\varphi),\ z = -(\tan\varphi)/\sqrt{48}. \quad (2)$$

To have a clear vision of the relationship between the octahedral-site rotation and lattice parameters, the primary rotation can be decomposed into two rotations around the 110 axis and the 001 axis of the primary cell or by the same decomposition locally in an octahedron as indicated by θ and ϕ in Fig.1(b). The rotation around ϕ (or 001) can change the overall dimension of the *ab* plane, but not the relationship between *a* and *b*. As shown in Fig.1(c), however, the rotation around θ, which is related to θ_1 in the overall crystal structure by $2\theta = 180-\theta_1$, enhances the buckling in the *ab* plane along the *a* axis and leads to $b > c/\sqrt{2} > a$. If rigid octahedra are assumed, a simulation using the software SPuDs [21] indicates that the relation $b > c/\sqrt{2} > a$ holds for *all values* of this rotation, yielding a smooth transition to the cubic structure. However, a crossover from $b > a$ to $b < a$ can be found in orthorhombic perovskite oxide systems as the *t* factor approaches 1 from $t < 1$ [22]. This apparent lattice parameter anomaly can be well explained by abandoning the rigid octahedra assumption and considering a specific octahedral-site distortion: a slight reduction from 90° in the O_{21}-Os-O_{22} bond angle, α, (open to the *a* axis) as shown in Fig.1(c). In this scenario, the reduction of the *a* axis due to the θ rotation is compensated by the now elongated octahedra along the *a* axis, which simultaneously reduces the *b* axis; the combination of these two changes eventually makes $a > b$. In summary, the behavior of *b-a* is controlled by both the octahedral-site distortion and the octahedral-site rotation in a *Pbnm* perovskite.

Returning to the temperature dependence of lattice parameters of $NaOsO_3$ in Fig.2, it is clear that the difference *b-a* increases significantly on cooling through T_{MIT}. The question is whether the

pronounced change of lattice parameters is due to a rigid octahedral change in the θ rotation or to an octahedral-site distortion as measured by the angle α or both. These two angles can be obtained directly from the refinement of neutron diffraction. Unfortunately, no clear changes of either of these two parameters can be discerned beyond the measurement uncertainty.

By taking advantage of the very high precision of the measured lattice parameters, the relative change of the octahedral rotation angle θ_l *in* Fig.1(a) on crossing T_{MIT} can be extracted through the formula $sin(\theta_l/2) \approx a/b$ if the octahedral-site rotation is the sole source for the change of lattice parameters, *i.e*. there is no octahedral distortion. Fig.3 displays the temperature dependencies of *b*-*a*, the directly measured value of θ_l from neutron data, and the simulated rotation angle θ_l derived from the lattice parameters. Corresponding to an abrupt increase of *b*-*a* on cooling through T_{MIT}, the simulated θ_l drops, indicating a more buckled *ab* plane. θ_l from the refinement of neutron diffraction differs from the simulated one by $\Delta\theta = 10°$ signaling that $sin(\theta_l/2) \approx a/b$ is oversimplified. However, the most important message is that the relative change of θ_l required to account for the change of *b*-*a* on cooling through T_{MIT} is clearly larger than the measurement uncertainty (the size of error bars in Fig.3(b)) of neutron diffraction. The absence of any change in the observed θ_l on cooling through T_{MIT} implies that the local structural change measured by the angle α, takes place at the transition.

Following the same protocol, we can simulate the primary rotation φ shown in Fig.1(b) based on the lattice parameters in a formula given by O'Keeffe and Hyde,[20]

$$\varphi = \cos^{-1}[\sqrt{2}a^2/(bc)] \quad (3)$$

again assuming the octahedra are perfectly regular. Fig.4(a) displays the simulated primary rotation, φ_{simu}, as derived from the measured lattice parameters, and the primary rotation calculated from the oxygen position determined by neutron diffraction through Eq.2, which is denoted as φ_O_{2z}. Again, the absolute difference between the two temperature dependencies of $\varphi(T)$ implies the octahedra are not perfectly regular. An obvious local distortion is that the angle α in Fig.1(c) deviates from 90°. Woodward *et al.* [23] have described the lattice parameter correction caused by this local distortion in the relationship

$$b/b_u = \sqrt{2}\sin\alpha;\ a/a_u = \sqrt{2}\cos\alpha \quad (4)$$

where a_u and b_u are for a cell with $\alpha = 90°$. We enter a_u and b_u of Eq.4 into Eq.3 and use α as a fitting parameter to make the φ_{simu} match with the observed $\varphi_{\_O2z}$. The results of forced matching between the two φ *(T)s* is shown along with φ_{simu} and $\varphi_{\_O2z}$ in Fig. 4a. The corresponding fitting parameter $\alpha_f(T)$ is displayed in Fig.4(b) with the measured valued of α(T). It is quite remarkable that the difference between the $\alpha_f(T)$ and the α(T) from neutron diffraction is within 0.15°. It implies that the site distortion α is a dominant octahedral-site distortion in $NaOsO_3$. The measurement uncertainty of the observed α(T) is too large to distinguish any change of α(T) at T_{MIT}. In contrast, the error bars for $\alpha_f(T)$ are smaller than the symbol size in the plot. The temperature dependence of α_f is significant and is the main result of this study; α_f appears to increase on cooling through T_{MIT}. The remaining question is whether the temperature dependence of α_f conveys any important message regarding an electronic structure change at T_{MIT}.

III. Correlation of local structural distortion and the orbital occupation

Before elaborating on the meaning of the change in α_f at T_{MIT}, it is useful to discuss octahedral-site distortions, as compared to rigid rotations, in perovskites. An $\alpha < 90°$ is commonly found in the *Pbnm* perovskite oxides where the octahedral-site tilting angles are relatively small and the *t* factor is close to 1 [22] . In the $RFeO_3$ family, for example, α starts to deviate from 90° for rare earths ions with an ionic radius (IR) larger than that of Gd. A progressive decrease of α continues as the IR further increases in the family; the total change of α from *R*=Gd to La is less than 1° [22]. The decrease of *b*-*a* from $GdFeO_3$ to $LaFeO_3$ results from a combination of the reduced octahedral-site rotation and the reduced angle α. The reduced octahedral-site rotation can explain a decrease of *b*-*a* as the *t* factor increases toward 1, but the change of rotation alone cannot account for *b*-*a* < 0 in the orthorhombic structure with rigid octahedra. For the perovskite families with the *t* factor approaching 1, such as in the series $RGaO_3$, $RCoO_3$, and $RNiO_3$, *b*-*a* < 0 indeed occurs, which directly illustrates the consequence of the octahedral-site distortion [22]. This intrinsic local distortion is in line with the theorem that "perfect regularity of the octahedra is incompatible with fixed rotation axes " [20]. For $NaOsO_3$, *t* =0.9989 is obtained by using SPuDs where the tabulated ionic radii (IR) of Na^+, Os^{5+}, and O^{2-} are used. Like other orthorhombic perovskites with *t* factor close to 1, a value of $\alpha_f(T) < 90°$ for $NaOsO_3$ for 360 < T < 490 K is

expected. To provide context for discussing whether an increase in α at the metal-insulator transition indicates a change of electronic structure, it is useful to examine other perovskite insulators over a wide range of temperature. $PrGaO_3$, which is a diamagnetic (from the Ga-O array) insulator and has been thoroughly studied by X-ray diffraction from 12 to 1200 K [24] and $PrNiO_3$ [25] which is metallic, are a nice examples. We again turn to the change of lattice parameters of these two perovskites. A detailed comparison of *b-a* for $NaOsO_3$ is given in Fig.3(a) and the same quantity for $PrGaO_3$ and $PrNiO_3$ is given in the insert. The linear increase of *b-a* as temperature decreases in insulating $PrGaO_3$ is comparable to that of $NaOsO_3$ at $T > T_{MIT}$. In the metallic $PrNiO_3$, *b-a* becomes negative and also changes linearly as temperature decreases. A negative *b-a* is indicative of an even larger octahedral-site distortion in metallic $PrNiO_3$ than that in the metallic phase of $NaOsO_3$; α is 88.5º at 300 K and reduced to 88.2º at 670 K in $PrNiO_3$. Interestingly, the slopes of fitting lines to the three sets of *b-a* (the data above T_{MIT} in $NaOsO_3$) in these perovskites are very close; it is $-3.8 * 10^{-5}$ Å/K for $NaOsO_3$, $-3.1 * 10^{-5}$ Å/K for $PrNiO_3$, and $-2.7 * 10^{-5}$ Å/K for $PrGaO_3$. An abrupt change of *b-a* on crossing T_{MIT} in $NaOsO_3$, then, must reflect a change of electronic behavior as even large distortions give rise to a smooth decrease if the electronic phase is constant.

Octahedral-site distortions in many cases reflect the orbital occupation. A typical example is the cooperative Jahn-Teller distortion as seen in $LaMnO_3$ where the electron occupation of the $3y^2$-r^2 and the $3x^2$-r^2 orbitals alternating in the lattice array of *ab* plane makes a distorted octahedral site with two long and four short bonds.[14] However, it has rarely been studied whether orbital occupation could change the bond angles in octahedra in the orthorhombic perovskites. In $NaOsO_3$, itinerant electrons in the π* band do not prefer any local bonding configuration. $NaOsO_3$ in the metallic phase above the transition adopts a crystal structure with intrinsic distortions like other orthorhombic perovskites, *i.e.* $\alpha < 90°$. However, localized electrons in t_{2g} orbitals would prefer a normal O_{21}-Os-O_{22}, *i.e.,* $\alpha = 90°$ and a normal O_1-Os-O_2 bond angle. Therefore, any transition from itinerant electrons to localized electrons on cooling through T_{MIT} would create a competing force against the intrinsic octahedral-site distortion. Since the connection between the lattice parameter difference *b-a* and the octahedral-site distortion described by α is well justified in the description above, we will consider the change of lattice parameters *b-a* instead of α (it is difficult to determine α precisely in a structural study) and its

connection to the orbital occupation in some well-known systems. In the case of σ* band electrons, the orbital ordering for the e_g electrons creates a bond-length distortion as well as the site preference for α =90°. The manganite $La_{1-x}Sr_xMnO_3$ has the same structure as $NaOsO_3$. Hole doping induces an evolution from an A-type antiferromagnetic insulator to a ferromagnetic metal. The coincident rapid shrinkage of *b*-*a* serves as a good indicator of how α deviates from 90°. Hole doping in the system reduces *b*-*a* due to the combination of a decreased octahedral-site rotation and α deviating from 90°. However, *b*-*a* < 0 is not allowed in the *Pbnm* structure with rotating rigid octahedra only. The cooperative Jahn-Teller bond distortion associated with Mn^{3+} in $La_{1-x}Sr_xMnO_3$ can influence the magnitude of *b*-*a*, but it maintains a positive value. The observation of *b* <*a* at some point of doping in the *Pbnm* $La_{1-x}Sr_xMnO_3$ reflects the deviation of α from 90°. An abrupt drop of *b*-*a* on passing a critical doping x=0.11 that separates the insulator and metallic phases in the system clearly indicates that electron localization in the e_g orbital in the insulator phase prefers an α close to 90° [26]. The stunningly similar behavior of *b*-*a* between the temperature-induced change in $NaOsO_3$ and the doping-induced change in $La_{1-x}Sr_xMnO_3$ suggests that electron localization occurs upon crossing T_{MIT} in $NaOsO_3$.

IV. Madelung Energy

In order to justify the relationship between the orbital occupation and the change of local structural distortion due to Coulomb interaction, we have calculated the Madelung energy in a point-charge model of the basal plane in an OsO_6 octahedron with an occupied xy orbital in Fig.5. The result clearly shows that the Madelung energy minimizes at α= 90°; it is clearly a driving force to compete with the intrinsic octahedral-site distortion with α< 90°. However, the angle dependence of the Madelung energy is extremely small; the difference is on the 4th decimal place. A more quantitative simulation of how a change of electronic behavior can influence the local structure is illustrated by the DFT calculations below, which includes the effects of Os-O hybridization missed in the point charge model.

V. DFT calculation

(1) Methods

All density functional theory calculations were performed with the Vienna Ab-Initio Simulation Program (VASP) [27] using the Projector Augmented Wave formulation [28] and the PBE

approximation to the exchange correlation functional [29]. To simulate localization, we applied several values of the Hubbard U parameter to the Os 5d orbitals using the rotationally invariant method of DFT+U [30]. For each value of U, we fully relaxed the structure, lattice constants and atomic positions, within the *Pbnm* space group. We used a dense k-point mesh of 12x9x12 and an energy cutoff of 500 eV. For the calculations with spin-orbit coupling (SOC), we used the non-collinear version of the VASP code, which treats the spin-orbit coupling with the second variational approach. For all cases, we established the spin-quantization axis along the *a*-axis which is experimentally known to be the easy axis. Attempts to establish a different easy axis were unsuccessful as the self-consistent result always ended up along the *a*-axis.

(2) Results

We used DFT to examine how SOC and varying values of localization (as manipulated by increasing U; see methods) affect the structure and electronic structure of $NaOsO_3$. We monitor both the gap opening at E_F via introduction of SOC and U, but also track the subtle changes of crystal structure on crossing the metal-insulator transition by fully relaxing both the lattice and atomic positions for each different U. We begin our calculation starting with the nonmagnetic state without SOC (State 1) and the nonmagnetic state with SOC (State 2). The electronic structure and density of states (DOS) obtained is similar to others reported in the literature.[10,11,12] Imposing the G-type AF spin order along with SOC, but without any correction to the GGA exchange correlation function (State 3) results in a deep pseudogap at E_F. This gap progressively widens to a true gap as the value of U is increased from 1 eV (State4) to 2 eV (State 5). The evolution of the DOS through the various described conditions is shown in Fig.6.

An analysis of the character of electronics states for U=2.0 eV with imposed G-type AFM ordering is shown in Fig.7. In this 5d transition-metal oxide, the exchange energy is smaller than the crystal field splitting. In $NaOsO_3$, with a formal $t_{2g}^3e_g^0$ configuration, the crystal field splitting separates the t_{2g} complex or π^* bands (~ -2 eV to 2 eV) from the e_g complex or σ^* bands (above 2 eV) leaving a gap of about 0.8 eV between the top of π^* band and the bottom of σ^* band. The exchange energy further splits the π^* manifold into an occupied spin-up complex and an empty spin-down complex. The interatomic interaction causes a spin mixture in the exchange-split occupied and empty complexes separated at E_F by the exchange energy and U. As shown in Fig.7, the occupied band includes a majority of spin-up states and significant portion of

spin-down states for the t_{2g} originated complex. The *p-d* hybridization is manifested by (1) a significant contribution of O-2p to the π^* band and (2) a nearly identical profile of N(E) for the t_{2g} and O-2p complex. However, the O-2p electrons are not spin polarized. The overlap of two spin bands and the *d-p* hybridization results in a reduced (from the formal 3 μ_B) moment of $\mu = \sim 1\ \mu_B$ on Os^{5+} from the self-consistent calculation, in good agreement with experiment.

As illustrated in Fig.5, the orbital occupation of the xy orbital has a strong influence on the bond angle α. Fig.8 displays the projected DOS of the three different orbitals of t_{2g} complex. They all share a similar profile without spin polarization, indicating approximately equal occupation. The G-type AFM ordering splits the complex and places E_F at the minimum of the total DOS, but the xy band now contributes the least to states at E_F and the bandwidth becomes the narrowest among three t_{2g} orbitals. These changes indicate that spin ordering and the easy axis due to the spin-orbit coupling (will be elaborated more below) allocates more electrons to the xy orbital than to the other two bands and that the xy orbital has the largest share of the total moment. Further increasing U opens a full gap, $\Delta = E_{ex} + U$, where E_{ex} is the exchange energy, which separates the majority up-spin band and majority down-spin band. The magnetic moment increases slightly along with the gap opening.

The calculated structural changes along with the evolution of the electronic states from State1 (U=0, non-magnetic, no SOC) to State5 (U=2, G-type AFM, applied SOC) are summarized in Fig.9. An increase in α progressing from State1 to State5 matches essentially that shown in Fig.4 (b) derived from the crystallographic model based on experimental data, and the absolute value of the calculated α is within 0.1° from the experimental result. This remarkably good agreement between simulation and experiment gives us confidence that we are capturing something important about the relevant physics and we proceed to analyze the electronic ramifications of these structural changes. It is interesting to note that the moment in these relaxed structures tracks closely the change of α through each of the five different states, which is consistent with the argument that restoring α toward to 90° is a consequence of the orbital occupation.

Before our in-depth examination of the structural and electronic changes across, T_{MIT}, we revisit the main relevant facts. Experiment shows that the *b*-axis suddenly increases while the *a*-axis decreases across the transition. Together these two changes cause overall no distinct change in the volume, although of course the volume is continuously decreasing with temperature due to

thermal contraction. We will argue that the sudden changes are the consequence of localization that sets in at T_{MIT}, triggering a change in the bond angle α. It is worth noting at this point that we force localization by manipulating the "U" in our calculations, but that there is no temperature since DFT is a ground state T=0 methodology. Therefore, the standard thermal contraction that can been seen in the data with decreasing temperature (and presumed increasing localization) will be missing from our results which are presented as increasing localization divorced from temperature.

Our calculations show that the *b*-axis increases whereas the *a*-axis remains unchanged on crossing from State1 to State5 in Fig.9. The overall change of *b*-*a* on crossing these electronic states matches very well with experimental data shown in Fig.3(a). To account for the absence of thermal effects as described above, we fit the temperature dependence of *b*-*a* in the phase above T_{MIT} to a line in Fig. 10. The negative slope of the temperature dependence of *b*-*a* in $NaOsO_3$ quantitatively matches that in $PrNiO_3$ and $PrGaO_3$ discussed above. The low-temperature extrapolation of the line to zero K hits the location of *b*-*a* for State1 surprisingly well. However, it is a long shot to predict the value of *b*-*a* at zero K based on the curve of *b*-*a* within a narrow temperature range for the phase below T_{MIT}. Nevertheless, as shown in Fig. 10, all of our reasonable guesses show it falling into a location covered by the five electronic states in the simulation. Therefore, the simulation of the five electronic states catches the essential structural changes on crossing the metal-insulator transition in $NaOsO_3$. Our calculations show that the *a*-axis value is essentially flat (although it reduces slightly from State3 to State4 in the low panel of Fig.9) across the different states of localization, as is observed in experiment on cooling through the metal insulator transition. However, the difference is small and is compensated by the overestimation of the increase in the *b* lattice parameter which brings *b*-*a* into good agreement with observation. The likely source of this systematic error is the known overestimation of lattice parameters in the GGA approximation which both exaggerates the *b* increase and suppresses the *a* decrease.

It is important to note that the monotonic increase of α along the evolution from itinerant to localized electronic behavior is not simply driven by minimizing the Coulomb energy while the xy orbital is increasingly occupied as indicated by the Madelung energy calculation or even by factoring in *p*-*d* directional hybridization. The spin-orbit coupling also plays a critical role. In

our relaxed calculations, the easy axis is found to be along the *a* axis, as is the experimental case without exception in G-type AFM *Pbnm* perovskites. Attempts to establish a different direction computationally were unsuccessful if the structure was allowed to relax. The trend of α is actually *opposite* if SOC is not included in the calculation, as is shown in the upper panel of Fig.9, underlining the importance of the spin-lattice coupling as a partial determining factor in the localization across the transition.

VI Discussion

(1) Electronic behavior revealed by the paramagnetic magnetic susceptibility.

Itinerant electrons in the Fermi sea become polarized under a magnetic field for a small portion of the density of states in the energy range of kT near the Fermi energy. The first term of thermodynamic expression of magnetic susceptibility for itinerant electrons gives a $\chi(T) \sim \mu_B^2 N(E_F)$, known as the Pauli formula.[31] In the extreme limit of localized electrons, *i.e.* isolated magnetic ions of in the gas phase, the magnetic moment is independent of temperature, which leads to the Curie law $\chi(T) = C/T$, where C is the Curie constant and can be related to the effective moment μ_{eff}. In a solid, exchange interactions lead to long range magnetic orderings, and the Curie law is reformulated as the Curie-Weiss (C-W) law, $\chi = C/(T-\Theta)$, where the Weiss constant can be related to the ordering temperature: $|\Theta| \sim T_N$ or T_c. The C-W law is valid only if fitting a $\chi(T)$ to the formula of C-W law gives a reasonable value of $|\Theta|$. Electron-electron correlations in metals such as $LaCuO_3$ and $LaNiO_3$ contribute a weak temperature dependence to the paramagnetic susceptibility [32]. Their inverse susceptibility, especially at high temperatures, can be closely fit to a line but this fitting yields a huge $|\Theta|$ and μ_{eff} in these paramagnetic metals. This kind of metal was studied in the 1970s and generally described as an enhanced Pauli paramagnetism [33] [34]. For itinerant electron systems with magnetic ordering, such as $ZrZn_2$ [35], a new C-W law proposed by Moriya should be applied.[36] The Curie constant, which is not relevant to μ_{eff} in this new law, is inversely proportional to the $N(E_F)$.

As mentioned in the introduction, fitting $\chi(T)$ in the paramagnetic phase of $NaOsO_3$ to a C-W law gives a $|\Theta|$=1949 K >> $T_N = T_{MIT}$ =410 K. This observation well qualifies the phase of $NaOsO_3$ above T_{MIT} as a correlation-enhanced Pauli metal like $LaNiO_3$ and $LaCuO_3$ and assigned as State1 (no SOC) or State2 (SOC) in our DFT calculation. The SOC effect on the paramagnetic susceptibility is to introduce the nonlinear behavior in the plot of inverse c versus

temperature,[37] [38] for example in 9R $BaRuO_3$.[39] The linear $\chi^{-1}(T)$ indicates a much weaker SOC effect in the paramagnetic state of $NaOsO_3$. Therefore, we could attribute the paramagnetic phase to State1. As detailed earlier, the overall change of α calculated for increasing localization as simulated by the electronic states from State1 to State5 matches that derived from the measured lattice parameters on crossing T_{MIT}. The overall change of magnetic moment from 0 to ~ 1 μ_B along with the increase of α is consistent with the electron localization and increased orbital occupation from the enhanced Pauli metal phase on cooling through T_{MIT}.

(2) The preferred local structure in the systems with no orbital degeneracy

The cooperative Jahn-Teller (JT) effect [40] is a structural instability connected to the lifting of an orbital degeneracy by the structural distortions in general and lowering the global symmetry in some cases. The JT effect is also accompanied by a dramatic change of physical properties such as a conductor-to-insulator transition in $LaMnO_3$ with the $t_{2g}^3e_g^1$ configuration [41]. $NaOsO_3$ has a $t_{2g}^3e_g^0$ configuration and adopts the orthorhombic perovskite structure having the intrinsic structural distortion exemplified by $LaGaO_3$ [42], a perovskite that has no orbital degeneracy or spin ordering, and an $\alpha < 90°$. Our DFT calculations show an electron density in the nonmagnetic metallic phase of $NaOsO_3$ (resembling the phase at $T > T_{MIT}$) as viewed by the isosurface plot around Os in an OsO_6 octahedron in Fig.11 (a). Whereas the isosurface still keeps the essential features of the electron distribution in the π^* band, the distortions reflect the strong hybridization between the d orbitals and the p orbitals in the oxide. The insulator phase with U=2.0 eV has an isosurface of electron density that has a more regular shape for the typical occupation of three t_{2g} orbitals. In addition, more charge density is moved away from the Os-O bonding directions to the area of xy, xz, yz orbitals. The change of charge density from the metallic phase to the insulator phase imposes a structural preference, *i.e.* an O-Os-O bond angle closing to 90° in an octahedron, as demonstrated by the point charge model in Fig.5. The structural preference due to the change of electronic state competes with the intrinsic structural distortion at T_{MIT} in $NaOsO_3$.

(3) Mott transition versus Slater transition

In his book,[43] Mott classified the Slater transition as an itinerant band analogue to a strong correlation-driven metal-insulator transition. In the picture of a Slater transition, electrons remain itinerant crossing the transition. The gap is opened at E_F which intercepts with the reduced Brillouin boundary due to a symmetry change associated with the AFM ordering. While it does

split the majority-spin occupied and the minority-spin empty bands, the antiferromagnetic ordering alone does not open up a clean gap at E_F in $NaOsO_3$ as indicated from the DFT calculation, shown as State 3 in Fig.6. We called the metal-insulator transition at T_{MIT} a muted Mott transition because of no obvious change in the cell volume at the transition. However, all other features of Mott physics stay, such as the occupation of atomic orbitals at $T < T_{MIT}$ and the correlation fluctuations at $T > T_{MIT}$. Clear evidence of the correlation fluctuations has been demonstrated in a RIXS experiment.[8 9] The structural study and the DFT calculations presented in this work show clear evidence of orbital occupation at $T < T_{MIT}$. It must be stressed that SOC also plays an important role in facilitating the muted Mott transition in $NaOsO_3$. The opening of a gap at the Fermi energy is not as simple as increasing U to a critical value as other DFT calculations in the literature.[10 11 12] Opening a gap at a U_c along with the particular structural change on crossing T_{MIT} in the orthorhombic $NaOsO_3$ can be simulated only if SOC and the correct easy axis are incorporated in the calculation. The magnetocrystalline single-ion anisotropy (MSIA) originates from spin-orbit coupling. In the case of $NaOsO_3$ (actually in all orthorhombic oxides with G-type AFM), MSIA places the easy axis of the moment along the *a* axis. The spin direction appears to facilitate an opening up of α which is also required by the electron occupation on the xy orbital.

VII Conclusion

The metal-insulator transition in the $NaOsO_3$ perovskite is not associated with a discontinuous change of the cell volume or change in crystal symmetry, but rather in a pronounced splitting of the lattice parameters *a* and *b* in the orthorhombic perovskite structure. There have been no attempts to elucidate the mechanism behind this change of lattice parameters or its effect on electronic structure. This work has correlated the change of lattice parameters with an octahedral-site distortion, parametrized by the bond angle α, which is commonly seen in the orthorhombic perovskite oxides. We subsequently correlate the change in α to changes in the electronic structure. This change has likely been previously missed due to its relative subtlety, but noting that α changes only about 1 degree from $LuFeO_3$ all the way to $LaFeO_3$, the change we find, $\Delta\alpha \approx 0.15$ degree, in a narrow temperature range around the metal-insulator transition in $NaOsO_3$ is dramatic. It reflects a structural change precipitated by the preference of localized electrons in conjunction with spin-orbit coupling, which competes with the intrinsic perovskite

structural distortion. The discovery of this local structural change suggests the metal-insulator transition found in the 5d transition-metal oxide $NaOsO_3$ cannot be fully attributed to the Slater mechanism; it should be treated as somewhat more closely associated with a Mott transition.

Acknowledgement

This work was primarily financially supported by the National Science Foundation through the Center for Dynamics and Control of Materials: an NSF MRSEC under Cooperative Agreement No. DMR-1720595 and DMR-2132574 and the Office of Naval Research through the U.S. Naval Research Laboratory Basic Science Program and the Summer Research Faculty Program. JSZ thanks S. Calder for providing the original cif files of the published neutron-diffraction data, and Kevin May and Bongjae Kim for useful discussions.

*jszhou@mail.utexas.edu

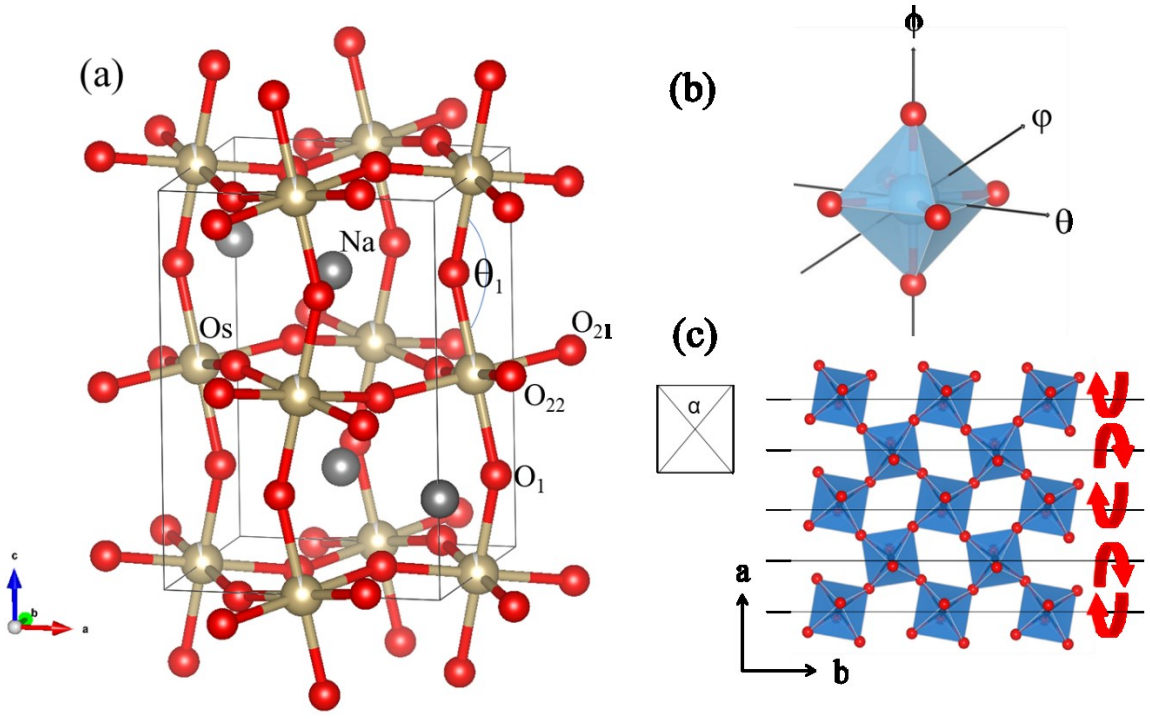

Fig.1 (a) The structural model of orthorhombic perovskite $NaOsO_3$. (b) An OsO_6 octahedron with three rotation axes. (c) The perovskite structure with OsO_6 octahedra projected onto the *ab* plane

from the *c* axis; the rotation around θ axis is indicated by red arrows. The rectangular box standing for exaggerated octahedra illustrates the bond angle α <90 °.

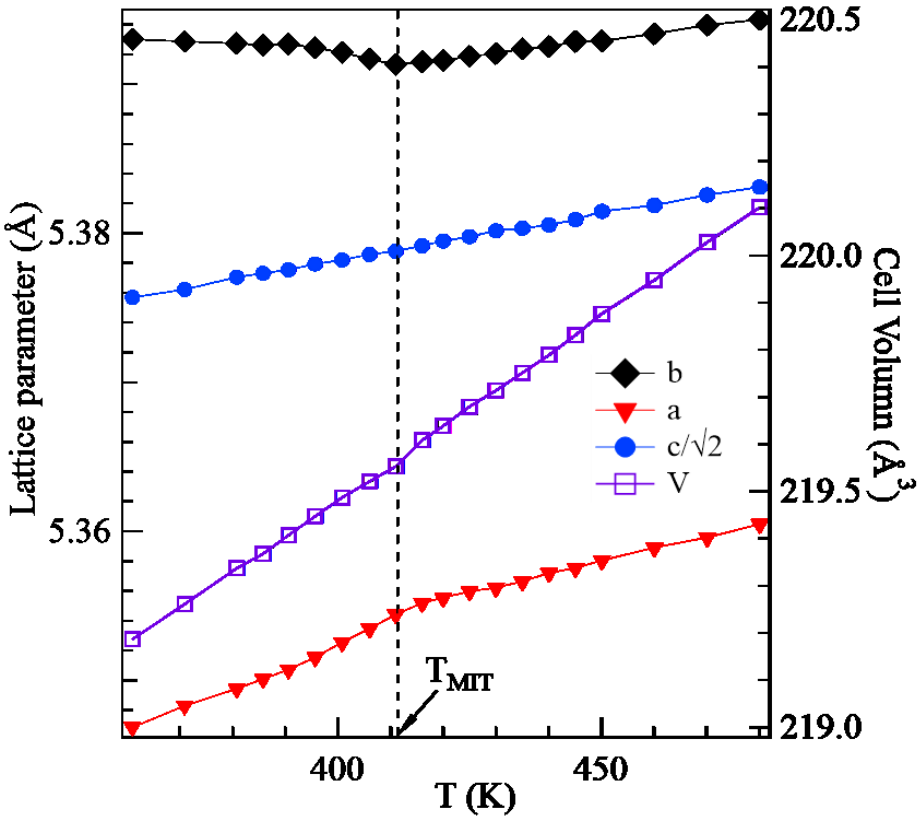

Fig.2 Temperature dependence of lattice parameters for $NaOsO_3$, data are after reference [2]. The error bars are smaller than symbols.

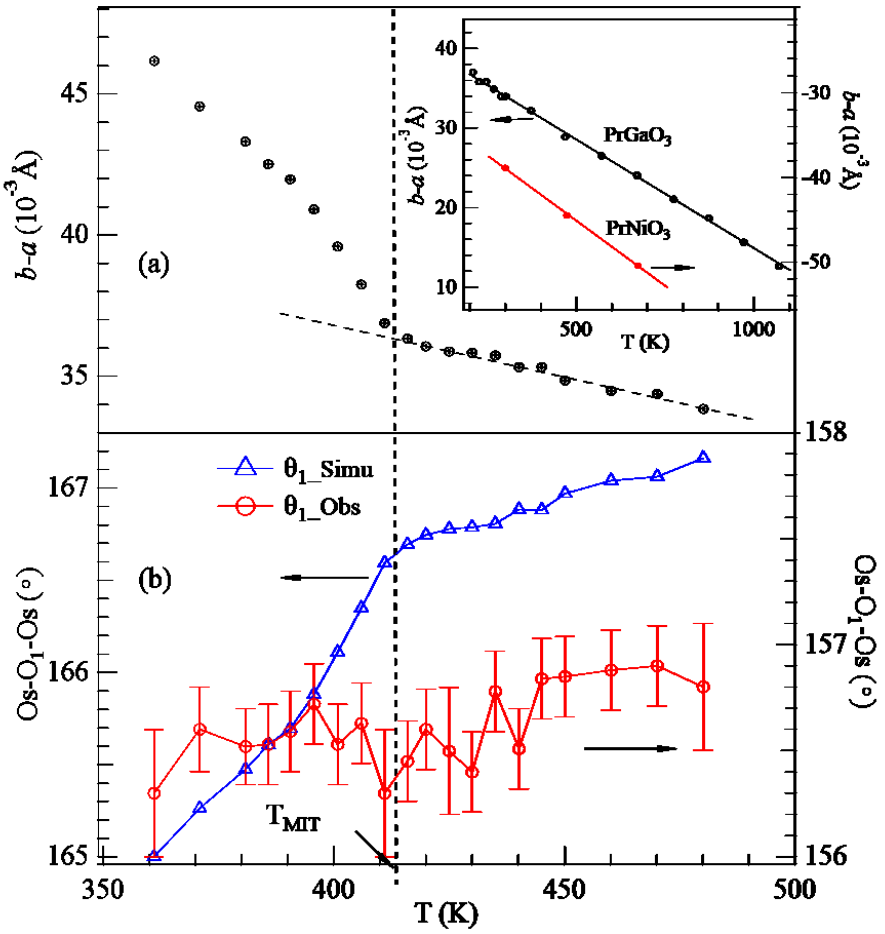

Fig.3 Temperature dependencies of (a) the difference of lattice parameters, *b-a,* of $NaOsO_3$ and $PrGaO_3$ and $PrNiO_3$ in the insert; (b) the simulated and the observed bond angle Os-O_1-Os in $NaOsO_3$.

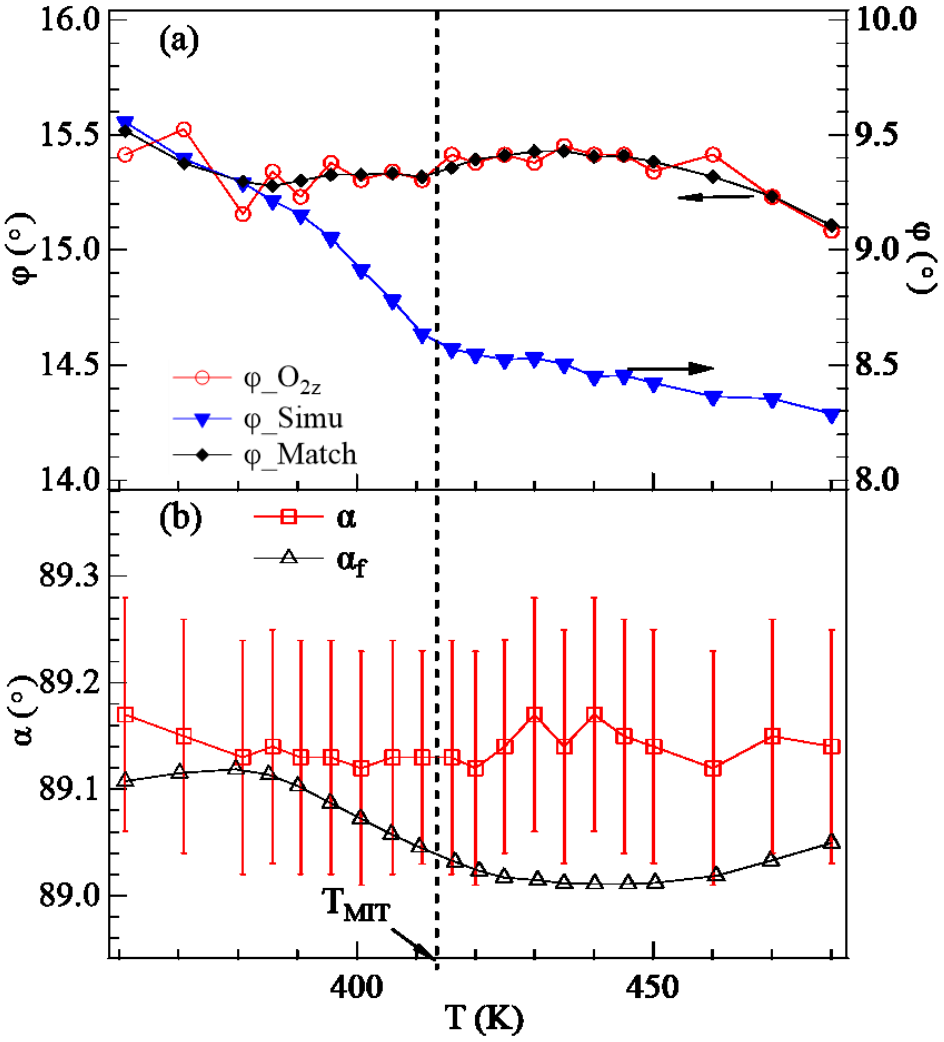

Fig.4 Temperature dependencies of (a) the primary rotation φ; (b) the O_{21}-Os-O_{22} bond angle α.

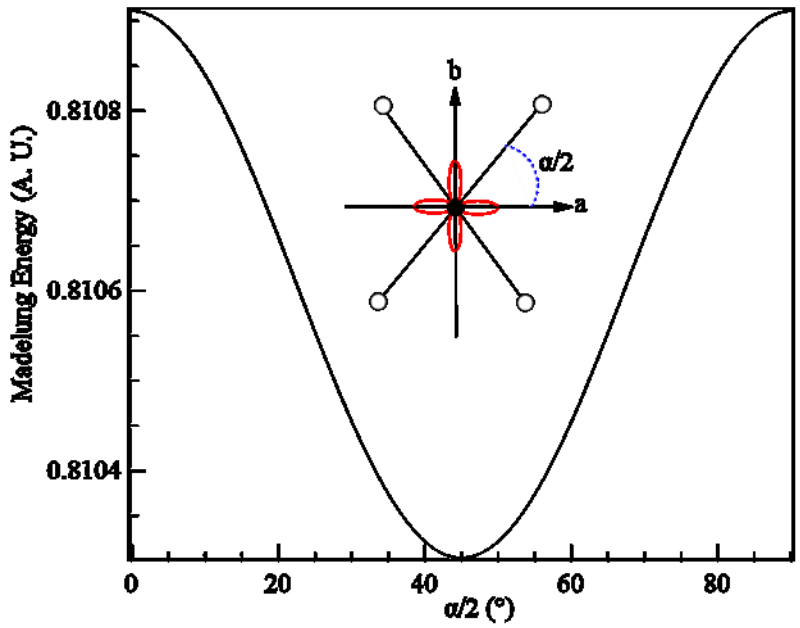

Fig.5. The Madelung energy in the *ab* plane of OsO_4 as a function of α/2.

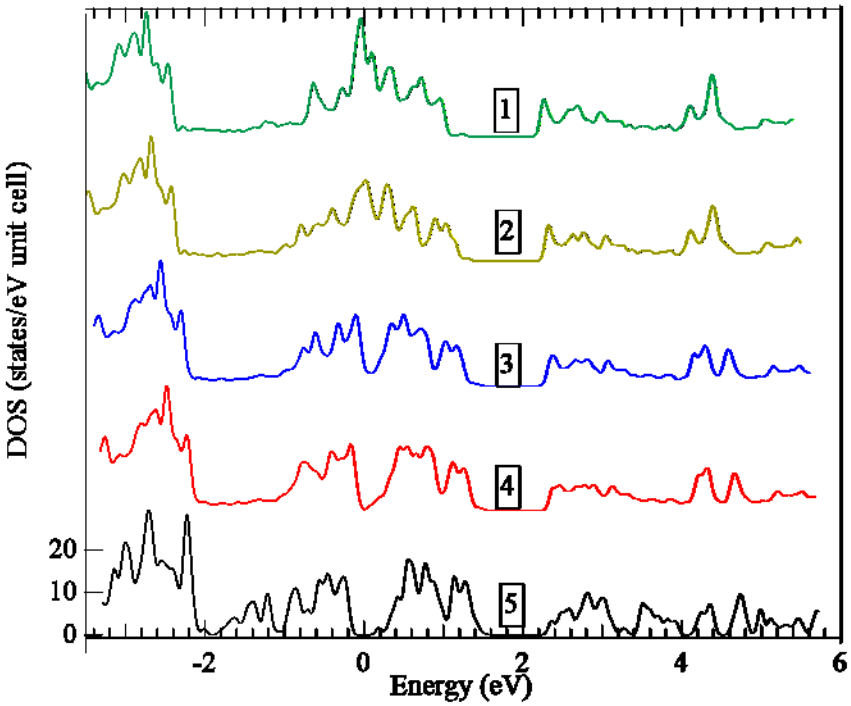

Fig.6 The density of states (DOS) of $NaOsO_3$ shown in the five investigated states (1) non-magnetic without SOC, (2) non-magnetic, including SOC (3) G-type AFM with SOC and U=0, (4) G-type AFM with SOC and U=1.0 eV (5) G-type AFM with SOC and U=2.0 eV

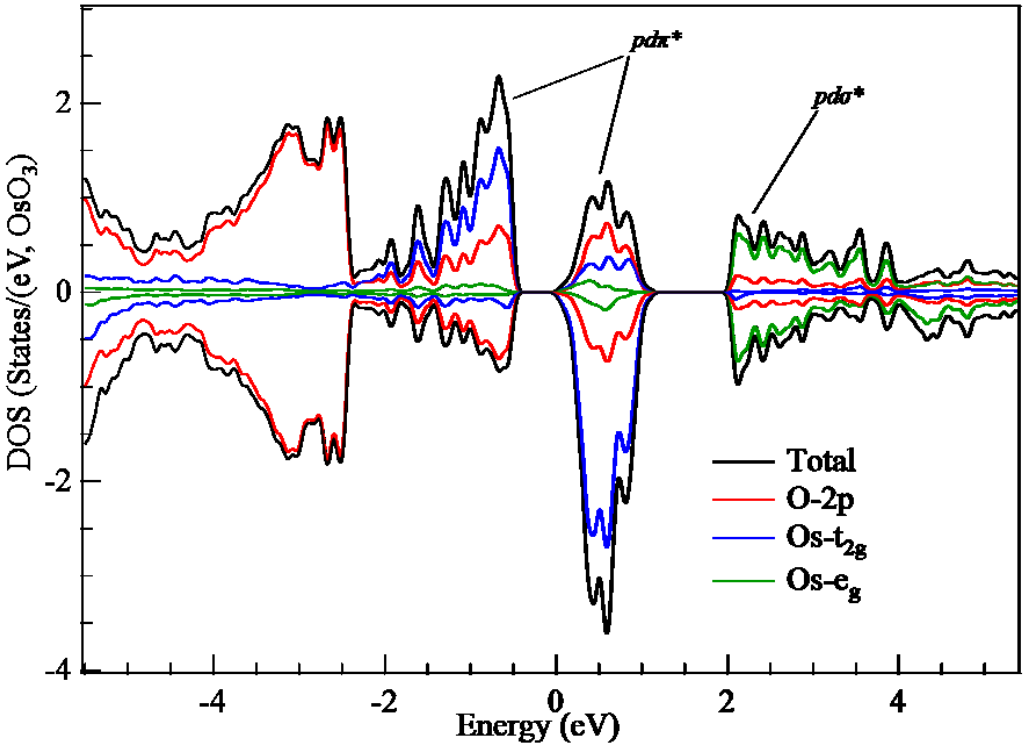

Fig.7 The density states of a specific Os-centered octahedron $OsO_{6/2}$ (majority spin "up") from the DFT calculation with G-AFM and U=2.0 eV without SOC. For this figure, the structure was rotated such that the Cartesian z-axis aligned with the c-axis of the system and the Cartesian x and y axes aligned with the bond configuration in the *ab* plane (a 45° rotation from the typical *Pbnm* structure) to allow a clean decomposition into t_{2g} and e_g manifolds. Adjacent octahedron would have identical DOS with "up" and "down" reversed.

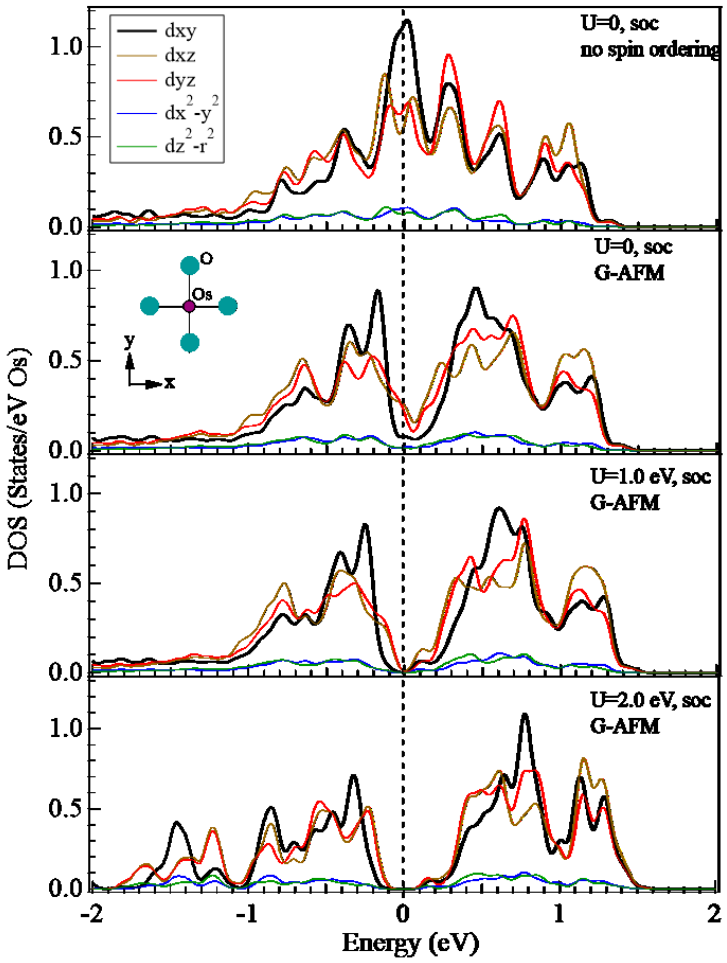

Fig.8 The DOS projected on the d orbitals for the five different electronic states simulated in $NaOsO_3$. For simplicity of comparison with and without spin-orbit, the DOS whether "up" and "down" (non-spin orbit) or in the various j (=l+s) (spin-orbit coupled) quantum states have been added together and plotted on the positive y-axis. The Cartesian x and y axes are the same as that in Fig.7 and illustrated in an insert plot.

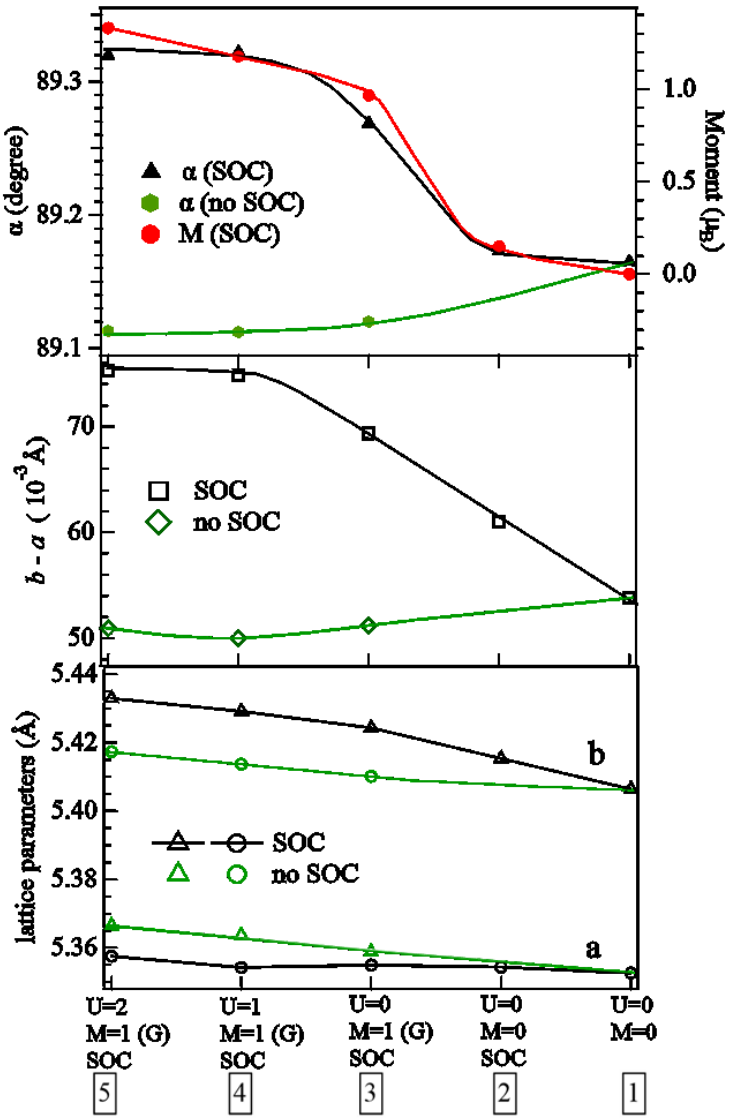

Fig.9 The structural parameters in the relaxed structures for different electronic states as labeled in the figure. The electronic states correspond to the DOS in Fig.6. Lines in the plots are guides to the eye.

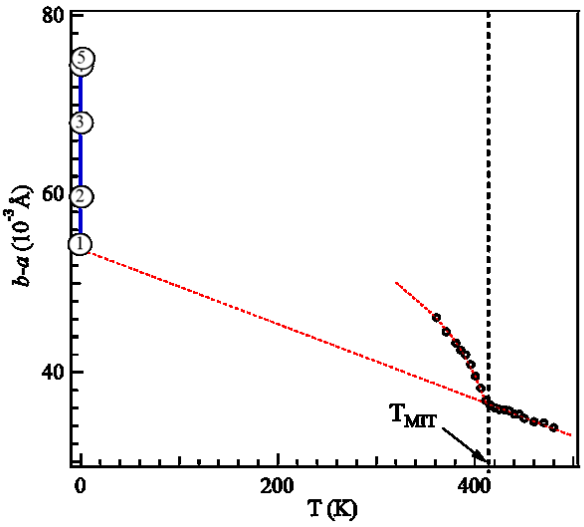

Fig.10 The temperature dependence of lattice parameters from experiment and the simulation results in this work.

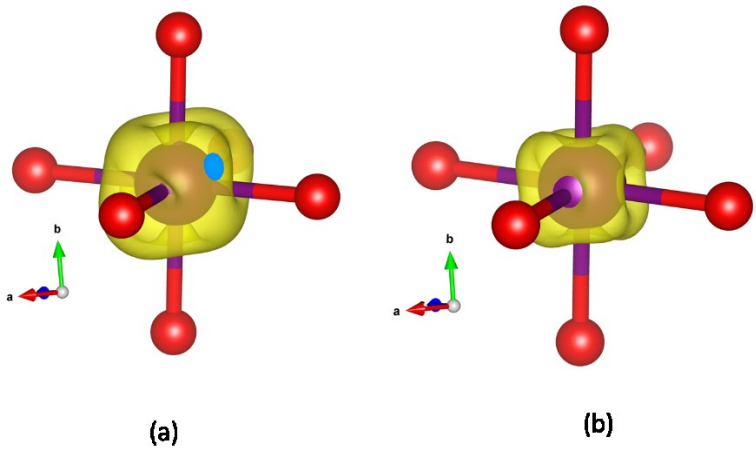

Fig.11 The isosurface (level=0.0043) of charge density distribution in an OsO_6 octahedron, (a) U=0 eV, SOC, M=0; (b) U=2.0 eV, SOC, M=1.

1 Y. G. Shi, Y. F. Guo, S. Yu, M. Arai, A. A. Belik, A. Sato, K. Yamaura, E. Takayama-Muromachi, H. F. Tian, H. X. Yang, J. Q. Li, T. Varga, J. F. Mitchell, and S. Okamoto, "Continuous metal-insulator transition of the antiferromagnetic perovskite NaOsO3 " Phys Rev B **80** (16), 161104R (2009).
2 S. Calder, V. O. Garlea, D. F. McMorrow, M. D. Lumsden, M. B. Stone, J. C. Lang, J. W. Kim, J. A. Schlueter, Y. G. Shi, K. Yamaura, Y. S. Sun, Y. Tsujimoto, and A. D. Christianson, "Magnetically Driven Metal-Insulator Transition in NaOsO3," Phys Rev Lett **108** (25), 257209 (2012).
3 J. S. Zhou, L.-P. Cao, J.A. Alonso, J. Sanchez-Benitez, M.T. Fernandez-Diaz, X. Li, J.-G. Cheng, L.G. Marshall, C.Q. Jin, and J. B. Goodenough, "Possible Bose-Einstein condensate associated with an orbital degree of freedom in the Mott insulator CaCrO3," Phys. Rev. B **94**, 155137 (2016).
4 T. Moriya, "Anisotropic Superexchange Interaction and Weak Ferromagnetism," Phys. Rev. **120**, 91 (1960).
5 N. Gurung, N. Leo, S. P. Collins, G. Nisbet, G. Smolentsev, M. Garcia-Fernandez, K. Yamaura, L. J. Heyderman, U. Staub, Y. Joly, D. D. Khalyavin, S. W. Lovesey, and V. Scagnoli, "Direct observation of electron density reconstruction at the metal-insulator transition in NaOsO3," Phys Rev B **98** (11), 115116 (2018).
6 J. C. Slater, "Magnetic Effects and the Hartree-Fock Equation," Physical Review **82** (4), 538-541 (1951).
7 I. Lo Vecchio, A. Perucchi, P. Di Pietro, O. Limaj, U. Schade, Y. Sun, M. Arai, K. Yamaura, and S. Lupi, "Infrared evidence of a Slater metal-insulator transition in NaOsO3," Scientific Reports **3**, 2990 (2013).
8 J. G. Vale, S. Calder, C. Donnerer, D. Pincini, Y. G. Shi, Y. Tsujimoto, K. Yamaura, M. M. Sala, J. van den Brink, A. D. Christianson, and D. F. McMorrow, "Evolution of the Magnetic Excitations in NaOsO3 through its Metal-Insulator Transition," Phys Rev Lett **120** (22), 227203 (2018).
9 J. G. Vale, S. Calder, C. Donnerer, D. Pincini, Y. G. Shi, Y. Tsujimoto, K. Yamaura, M. M. Sala, J. van den Brink, A. D. Christianson, and D. F. McMorrow, "Crossover from itinerant to localized magnetic excitations through the metal-insulator transition in NaOsO3," Phys Rev B **97** (18), 184429 (2018).
10 Y. P. Du, X. G. Wan, L. Sheng, J. M. Dong, and S. Y. Savrasov, "Electronic structure and magnetic properties of NaOsO3," Phys Rev B **85** (17), 174424 (2012).
11 B. Kim, P. T. Liu, Z. Ergonenc, A. Toschi, S. Khmelevskyi, and C. Franchini, "Lifshitz transition driven by spin fluctuations and spin-orbit renormalization in NaOsO3," Phys Rev B **94** (24), 241113R (2016).
12 M. C. Jung, Y. J. Song, K. W. Lee, and W. E. Pickett, "Structural and correlation effects in the itinerant insulating antiferromagnetic perovskite NaOsO3," Phys Rev B **87** (11), 115119 (2013).
13 S. Middey, S. Debnath, P. Mahadevan, and D. D. Sarma, "NaOsO3: A high Neel temperature 5d oxide," Phys Rev B **89** (13), 134416 (2014).
14 J. S. Zhou and J. B. Goodenough, "Unusual evolution of the magnetic interactions versus structural distortions in RMnO3 perovskites," Phys Rev Lett **96** (24), 247202 (2006).
15 G.G. Guzman-Verri, R.T. Brierley, and P.B. Littlewood, "Cooperative elastic fluctuations provide tunning of the metal-insulator transition," Nature **576**, 429 (2019).
16 M. Imada, A. Fujimori, and Y. Tokura, "Metal-insulator transitions," Reviews of Modern Physics **70** (4), 1039-1263 (1998).
17 J. B. Torrance, P. Lacorre, A. I. Nazzal, E. J. Ansaldo, and C. Niedermayer, "Systematic Study of Insulator-Metal Transitions in Perovskites Rnio3 (R = Pr, Nd, Sm, Eu) Due to Closing of Charge-Transfer Gap," Phys Rev B **45** (14), 8209-8212 (1992).
18 J. S. Zhou, J. B. Goodenough, B. Dabrowski, P. W. Klamut, and Z. Bukowski, "Enhanced susceptibility in LNiO3 perovskites (L = La, Pr, Nd, Nd0.5Sm0.5)," Phys Rev Lett **84** (3), 526-529 (2000).

19 J. S. Zhou, J. B. Goodenough, and B. Dabrowski, "Exchange interaction in the insulating phase of RNiO3," Phys Rev Lett **95** (12), 127204 (2005).
20 M. Okeeffe and B. G. Hyde, "Some Structures Topologically Related to Cubic Perovskite (E21), Reo3 (Do9) and Cu3au(L12)," Acta Crystallographica Section B-Structural Science **33** (Dec), 3802-3813 (1977).
21 M. W. Lufaso and P. M. Woodward, "Prediction of the crystal structures of perovskites using the software program SPuDS," Acta Crystallographica Section B-Structural Science **57**, 725-738 (2001).
22 J. S. Zhou and J. B. Goodenough, "Universal octahedral-site distortion in orthorhombic perovskite oxides," Phys Rev Lett **94** (6), 065501 (2005).
23 P. M. Woodward, T. Vogt, D. E. Cox, A. Arulraj, C. N. R. Rao, P. Karen, and A. K. Cheetham, "Influence of cation size on the structural features of Lu(1/2)A(1/2)MuO(3) perovskites at room temperature," Chemistry of Materials **10** (11), 3652-3665 (1998).
24 L. Vasylechko, Ye Pivak, A. Senyshyn, D. Savytskii, M. Berkowski, H. Borrmann, M. Knapp, and C. Paulmann, "Crystal structure and thermal expansion of PrGaO3 in the temperature range 12–1253K," Journal of Solid State Chemistry **178** (1), 270-278 (2005).
25 T. C. Huang, W. Parrish, H. Toraya, P. Lacorre, and J. B. Torrance, "High-temperature crystal structures of orthorhombic and rhombohedral PrNiO3," Mater Res Bull **25** (9), 1091-1098 (1990).
26 J. S. Zhou and J. B. Goodenough, "Local structural distortions, orbital ordering, and ferromagnetism in underdoped La1-xSrxMnO3," Phys Rev B **91** (6), 064414 (2015).
27 G. Kresse and J. Hafner, "Ab initio molecular dynamics for liquid metals," Phys Rev B **47** (1), 558-561 (1993).
28 P. E. Blöchl, "Projector augmented-wave method," Phys Rev B **50** (24), 17953-17979 (1994).
29 John P. Perdew, Kieron Burke, and Matthias Ernzerhof, "Generalized Gradient Approximation Made Simple," Phys Rev Lett **77** (18), 3865-3868 (1996).
30 S. L. Dudarev, G. A. Botton, S. Y. Savrasov, C. J. Humphreys, and A. P. Sutton, "Electron-energy-loss spectra and the structural stability of nickel oxide: An LSDA+U study," Phys Rev B **57** (3), 1505-1509 (1998).
31 C. Kittel, *Introduction to Solid State Physics, 7th edition*. (John Wiley and Sons, 1996).
32 J. S. Zhou, L. G. Marshall, and J. B. Goodenough, "Mass enhancement versus Stoner enhancement in strongly correlated metallic perovskites: LaNiO3 and LaCuO3," Phys Rev B **89** (24), 245138 (2014).
33 G. Demazeau, A. Marbeuf, M. Pouchard, P. Hagenmuller, and J. B. Goodenough, C.R. Acad. Sci. **272** (2163) (1971).
34 J. B. Goodenough, N.F. Mott, M. Pouchard, and G. Demazeau, Mat. Res. Bull. **8** (647) (1973).
35 Shinji Ogawa and Nobuhiko Sakamoto, "Magnetic Properties of ZrZn2–Itinerant Electron Ferromagnet," Journal of the Physical Society of Japan **22** (5), 1214-1221 (1967).
36 T. Moriya, *Electron Correlation and magnetism in Narrow-band Systems*. (Springer-Verlag, Berlin, 1981).
37 Junjiro Kanamori, "Theory of the Magnetic Properties of Ferrous and Cobaltous Oxides, I," Progress of Theoretical Physics **17** (2), 177-196 (1957).
38 Junjiro Kanamori, "Theory of the Magnetic Properties of Ferrous and Cobaltous Oxides, II," Progress of Theoretical Physics **17** (2), 197-222 (1957).
39 Marc Drillon, Lilijane Padel, and Jean-Claude Bernier, "Effects of spin–orbit coupling and exchange in BaRuO3," Journal of the Chemical Society, Faraday Transactions 2: Molecular and Chemical Physics **75** (0), 1193-1198 (1979).
40 J. B. Goodenough, *Magnetism and the Chemical Bond*. (John Willey and Sons, New York, 1963).

41 J. S. Zhou and J. B. Goodenough, "Paramagnetic phase in single-crystal LaMnO3," Phys Rev B **60** (22), R15002-R15004 (1999).
42 M. Berkowski, J. Fink-Finowicki, P. Byszewski, R. Diduszko, E. Kowalska, R. Aleksiyko, W. Piekarczyk, L. O. Vasylechko, D. I. Savytskij, L. Perchuć, and J. Kapuśniak, "Growth and structural investigations of La1−xPrxGaO3 solid solution single crystals," Journal of Crystal Growth **222** (1), 194-201 (2001).
43 N.F. Mott, *Metal-Insulator Transitions*. (Yaylor and Francis, London, 1990).